1
Electronic Transport and Optical Properties of Graphene

Klaus Ziegler, Antonio Hill, and Andreas Sinner

1.1
Introduction

The enormous list of publications on transport measurements in graphene starts with the seminal papers by the groups from Manchester and Columbia [1a]. Already these studies indicated a very robust transport behavior, which is characterized by a "V"-shaped conductivity with respect to charge density n and a minimal conductivity $\sigma_{\min} \approx 4e^2/h$ at the charge neutrality point $n = 0$. In the presence of a magnetic field, there are Shubnikov–de Haas oscillations for the longitudinal conductivity σ_{xx} and quantum Hall plateaux for the Hall conductivity σ_{xy} at a sufficiently strong magnetic field. These properties have been confirmed subsequently by various experimental groups in more detailed studies and measurements under various conditions and for different types of samples. Many of those results are collected and discussed in a number of extensive reviews [2–4].

Optical properties of graphene for light with frequency ω are (directly) related to the optical (or AC) conductivity $\sigma_{xx}^{\mathrm{AC}}(\omega)$. The imaginary part of the dielectric constant is related to the real part of the AC conductivity and, therefore, to the optical reflectivity and transmittance [5].

The aim of this chapter is to explain how the transport properties are related to fundamental physical principles, and we will focus on transport in the absence of a magnetic field. Transport in metals is based on the assumption that the charge carriers are Fermionic quasiparticles. The quasiparticles scatter on each other and on the impurities or defects of the underlying lattice structure. This represents a complex dynamical system which can be treated in practice only under some simplifying assumptions. First, we consider only independent quasiparticles of the system and average over all possible scattering effects. For the latter, we introduce a static distribution by assuming that the relevant scattering processes happen only on time scales that are large in comparison with the tunneling process of the quasiparticle in the lattice. In other words, the probability for the quasiparticle to move from site $\mathbf{r}'$ to site $\mathbf{r}$ during the time t is $P_{\mathbf{r}\mathbf{r}'}(t) = |\langle \mathbf{r}| \exp(-iHt)|\mathbf{r}'\rangle|^2$, where H is the hopping Hamiltonian. Second, if we assume that $P_{\mathbf{r}\mathbf{r}'}(t)$ describes

Graphene Optoelectronics: Synthesis, Characterization, Properties, and Applications. First Edition.
Edited by A. Rashid bin Mohd Yusoff.

diffusion, we can obtain the mean-square displacement with respect to $\mathbf{r}' = 0$ from the diffusion equation

$$\langle r_k^2 \rangle = \sum_{\mathbf{r}} r_k^2 P_{\mathbf{r},0}(t) = Dt \tag{1.1}$$

Using the Green's function $G_{\mathbf{r}\mathbf{r}'}(z) = (H - z)^{-1}_{\mathbf{r}\mathbf{r}'}$, we obtain the diffusion coefficient at energy E as

$$D(E) \sim \lim_{\epsilon \to 0} \epsilon^2 \sum_{\mathbf{r}} r_k^2 \langle G_{\mathbf{r}0}(E + i\epsilon) G_{0\mathbf{r}}(E - i\epsilon) \rangle_d \tag{1.2}$$

where $\langle ... \rangle_d$ is the average with respect to the disorder that is causing scattering, and E_0 is the lower band edge. Then the diffusion coefficient in Equation 1.1 is related to $D = \int_{E_0}^{E_F} D(E) \mathrm{d}E$. For transport in graphene at low temperatures, we need the diffusion coefficient only at the Fermi energy E_F.

A quantum approach to transport starts from a Hamiltonian H (here for independent electrons) and the corresponding current operator, expressed by the commutator

$$j_k = -ie[H, r_k] \tag{1.3}$$

where r_k is a component of the position operator of the electron. The average current induced by a weak external electric field E is obtained in terms of linear response as Ohm's law

$$\langle j_k \rangle = \sigma_{kl} E_l \tag{1.4}$$

with conductivity σ_{kl}. The general form of the conductivity in the Kubo formalism can be expressed as a product of one-particle Green's functions $G(z)$ at different energies z [6]. In the following, we exclude an external magnetic field. This leads to a vanishing Hall conductivity $\sigma_{kl} = 0$ for $k \neq l$. Then we can distinguish transport in a field which is constant in time, described by the DC conductivity σ^{DC}, and transport in an oscillating field $E(t) = E_0 \cos \omega t$, described by the optical or AC conductivity σ^{AC}. These two types of conductivities are discussed briefly in the remainder of this chapter.

DC conductivity: The DC conductivity σ at temperature $T \sim 0$ can be calculated either from D via the Einstein relation as $\sigma \propto \rho(E_F) D(E_F)$ with the density of states ρ, or from linear response theory via the Kubo formula [3, 7]

$$\sigma_{\mathrm{DC}} = -\frac{e^2}{\hbar} \lim_{\omega, \delta \to 0} \omega^2 \sum_{\mathbf{r}} r_k^2 Tr_2 \langle G_{\mathbf{r}0} \left(E_F + \frac{\hbar\omega}{2} + i\delta \right) G_{0\mathbf{r}} \left(E_F - \frac{\hbar\omega}{2} - i\delta \right) \rangle_d \tag{1.5}$$

where Tr_2 is the trace with respect to the Pauli matrices. The latter expression is obviously related to the diffusion equation in Equation 1.2 by the analytic continuation $i\epsilon \to \hbar\omega/2 + i\delta$. Thus the main goal for the DC transport calculation is to evaluate the average product of the Green's functions in Equations 1.2 and 1.5.

AC conductivity: In contrast to the DC conductivity, where the diffusion on arbitrarily large scales dominates the conductivity, the AC conductivity at frequency ω has the maximum length scale $L_\omega = v_F/\omega$, which is the wavelength corresponding to the Fermi velocity v_F. This means that all physical processes appear as if the system were restricted to a finite length L_ω. This fact simplifies the transport

calculations substantially. The drawback of the finite cutoff L_ω, however, is that we cannot approximate the AC transport by the asymptotic behavior for large scales, as in Equation 1.2, but we need to include the details on finite scales. Then the real part of the optical conductivity at temperature $T = 1/k_B\beta$ reads [6]

$$\sigma_{AC,\mu\mu}(\omega) = \frac{i}{\hbar}\int_{-\infty}^{\infty}\int_{-\infty}^{\infty}\langle Tr\left(j_\mu\delta(H-E-\hbar\omega)j_\mu\delta(H-E)\right)\rangle_d \frac{1}{E-E'+\hbar\omega+i0^+}\frac{f_\beta(E')-f_\beta(E)}{E-E'}dEdE' \tag{1.6}$$

with the Fermi–Dirac distribution $f_\beta(E) = [1+\exp(\beta(E-E_F))]^{-1}$ and the current operator $j_\mu = -ie[H, r_\mu]$. Moreover, we have used the trace Tr with respect to real space and spinor components. The Dirac delta function can be expressed by the Green's function as

$$\delta(H-z) = \frac{-i}{2\pi}\left[G(z+i\delta) - G(z-i\delta)\right]$$

Equations 1.5 and 1.6 are the basic formulas that will be used for the subsequent discussion of electronic transport and optical properties in graphene.

Before we start our survey on the properties of graphene, we briefly recall what is known about the transport properties of conventional metals. To a good approximation, the DC and AC conductivities are described by the Drude formula

$$\overline{\sigma}_{DC} = \frac{ne^2\tau}{m}, \quad \overline{\sigma}_{AC}(\omega) = \frac{\overline{\sigma}_{DC}}{1-i\omega\tau} \tag{1.7}$$

where τ is the scattering time, m is the quasiparticle mass, and n the charge density. These parameters are given as model parameters for the specific material. These classical approximations are not valid in the case of graphene, though, neither for monolayer graphene (MLG) nor for bilayer graphene (BLG). Hwang *et al.* applied the Boltzmann approach to the effective scattering time [8]. It reproduces the experimental results at high charge densities (far away from the Dirac node) but also gives $\sigma_{min} = 0$, like the conventional Boltzmann approach.

There are only two parameters, besides the frequency ω and the particle mass m, namely the scattering time τ (or the related scattering rate $\eta = \hbar/\tau$) and the carrier density n, which determine the transport properties. This is also the case for graphene, as we will explain in the following. For this discussion, the expressions 1.2, 1.5, and 1.6 are the fundamental quantities for the subsequent discussion of MLG and BLG. Here, it should also be mentioned that in MLG the charge density n is proportional to E_F^2, in contrast to the linear relation in conventional metals. This is a consequence of the linear density of states.

1.2 Basic Experimental Facts

Before we embark on the theory of transport in graphene, we briefly summarize the experimental observations that are relevant for the subsequent theoretical part.

Already the first experiments on graphene by Novoselov *et al.* [1b] and Zhang *et al.* [1c] revealed very characteristic transport properties in graphene. Graphene as well as a stack of two graphene sheets (graphene bilayer) are semimetals with remarkably good conducting properties [1b–9]. These materials have been experimentally realized with external gates, which allow a continuous change of the charge carrier density. It was found that the longitudinal conductivity changes linearly as a function of charge density with a negative slope for holes and a positive slope for electrons, showing a characteristic "V"-shaped behavior. Moreover, there is a minimal conductivity $\sigma_{\min}$ near the charge neutrality point. The latter has attracted some attention because it is unexpected in terms of the classical Boltzmann approach, and its value seems to be quite robust with respect to the sample quality and temperature [9–12]. More recent experiments by the group of *E.* Andrei on suspended graphene [13], however, indicated that, below $T \approx 150$ K, the minimal conductivity decreases linearly with decreasing T and reaches the extrapolated value $\sigma_{\min} \approx 2e^2/h$ at $T = 0$. A similar result was found by Danneau *et al.* [14]. This clearly indicates that the main mechanism of transport in graphene at the nodal point is diffusion, possibly with a crossover to ballistic transport due to a very large mean free path $L_s = v_F\tau$ of several hundred nanometers. Away from the charge neutrality point, the linear behavior has not always been observed but a crossover to a sublinear behavior for decreasing temperatures [13].

Role of disorder—Disorder plays an important role in the physics of graphene. First of all, a two-dimensional lattice is thermodynamically unstable. It is known that this is the origin of the strong corrugations in graphene in the form of ripples. Another source of disorder is impurities in the substrate, which probably affect the transport properties substantially. Recent experiments on suspended graphene and with clean substrates have been able to eliminate this type of disorder. Experimental evidence of the strong effects of disorder comes from the observation of puddles of electrons and holes at the charge neutrality point [15]. Experiments with hydrogenated graphene (graphane), where disorder is added by an inhomogeneous coverage with hydrogen atoms, lead to the formation of localized states which causes a nonmetallic behavior characterized by a variable-range hopping conductivity [16].

Role of electron–electron interaction—There is no clear evidence for a substantial effect of electron–electron interaction on the transport properties. Coulomb interaction renormalizes the Fermi velocity logarithmically near the Dirac point. But this only weakly affects the transport because the Fermi velocity drops out of the Kubo formula near the Dirac node. This is also supported by theoretical findings, based on perturbative renormalization group calculations [17–20], that Coulomb interaction provides only a correction of 1–2% for the optical conductivity [21]. This is in good agreement with experiments on the optical transparency of graphene [22, 23].

Role of electron–phonon interaction–Although there is substantial electron–phonon interaction in graphene [24–26], its effect on the transport properties has not been investigated in detail. Some experimental findings of a gap opening was associated with electron–phonon interaction [27] but in most samples

Table 1.1 Measured values of the scattering time τ and the Fermi energy in graphene and related quantities.

Quantity	Relation	Measured values in [28]	Typical values [10]
Scattering time τ	—	$0.36-1.08\ 10^{-14}$ s	$10^{-14}-10^{-12}$ s
Scattering rate η	$\hbar/\tau$	6–18 meV	0.7–70 meV
Scattering length L_s	$v_F\tau$	40–100 nm	10–100 nm
Diffusion coefficient D	$v_F^2\tau/2$	18–50 cm^2/s	50–5000 cm^2/s
Fermi energy E_F	—	−200–0 meV	−10–10 meV

the conductivity is explained by noninteracting particles. The optical conductivity might be affected by electron–phonon interaction of gated graphene before interband scattering can dominate the transport (i.e., when the frequency ω is less than $E_F/\hbar$) [23].

An important question is how τ depends on the Fermi energy E_F. Its frequency dependence was measured as $\tau = 10^{-14}-10^{-12}$ s [10] and was almost constant ($\tau \approx 10^{-14}$ s in Ref. [28]). In Table 1.1, we have collected some measured values of the scattering time τ and the Fermi energy E_F in graphene. The corresponding values of the scattering rate and the scattering length are calculated. The diffusion coefficient is calculated from its weak-localization form. It should be noticed that this is only a rough estimate for D, as we will explain in Section 1.4.

The experimentally measured DC conductivity as a function of the (electron or hole) charge density n is well explained by the empirical formula

$$\sigma_{DC}(n) = \sigma_{\min} + e\mu n \tag{1.8}$$

where μ is the mobility, which is related to the scattering time by $\mu = ev_F^2\tau/E_F$. Comparing this expression with the Drude formula (Equation 1.7), we observe that in the latter $\sigma_{\min} = 0$ and the mass is replaced by $m \to E_F/v_F^2$.

1.3 Models for Transport in Graphene

In order to calculate the conductivities (1.5) and (1.6), we must specify the Hamiltonians for MLG and BLG, where we focus on the low-energy properties near the nodes of neutral graphene. An important aspect is to take into account random scattering caused by ripples and impurities. Moreover, a random gap can appear as a result of local impurities. For instance, in the case of MLG, such local fluctuations appear in the coverage of MLG by additional non-carbon atoms [16, 29]. In the case of BLG with a dual gate [30, 31], the random gap is caused by the fact that the graphene sheets are not planar but create ripples [2, 32, 33]. As a result, electrons experience a randomly varying gap along each graphene sheet.

The two bands in MLG and the two low-energy bands in BLG represent a spinor-1/2 wave function. This allows us to expand the corresponding Hamiltonian $H = H_0 + V$ in terms of Pauli matrices σ_j as

$$H_0 = h_1\sigma_1 + h_2\sigma_2, \quad V = \sum_{j=0}^{3} v_j\sigma_j. \tag{1.9}$$

Near each node, the coefficients h_j in the low-energy approximation read [34]

$$h_j = p_j \quad \text{(MLG)}, \quad h_1 = p_1^2 - p_2^2, \quad h_2 = 2p_1p_2 \quad \text{(BLG)} \tag{1.10}$$

with momentum p_j. This is a momentum expansion of the tight-binding Hamiltonians around the nodes K and K′.

For randomness, it is assumed here that scattering appears only at small momentum such that intervalley scattering, which requires a large momentum at least near the nodes, is not relevant and can be treated as a perturbation. Then each valley contributes separately to the density of states and to the conductivity, and the contributions of the two valleys add. This allows us to consider the low-energy Hamiltonian in Eqs. (1.9) and (1.10) for each valley separately, even in the presence of randomness. Within this approximation, the gap term $v_3 \equiv m$ is a random variable. The following analytic calculations will be based entirely on the Hamiltonian of Eqs. (1.9) and (1.10). In particular, the average Hamiltonian $\langle H\rangle$ can be diagonalized by Fourier transformation and becomes a two-dimensional Dirac Hamiltonian for MLG

$$H_M \equiv \langle H\rangle = p_1\sigma_1 + p_2\sigma_2 + m\sigma_3 \tag{1.11}$$

with eigenvalues $E_p = \pm\sqrt{m^2 + p^2}$. For BLG, the average Hamiltonian is

$$H_B \equiv \langle H\rangle = (p_1^2 - p_2^2)\sigma_1 + 2p_1p_2\sigma_2 + m\sigma_3 \tag{1.12}$$

with eigenvalues $E_p = \pm\sqrt{m^2 + p^4}$. In order to apply the results from these calculations to the real materials, we must include a degeneracy factor $\gamma = 4$, referring to the two valleys K and K′ and the two-fold spin degeneracy of the electrons.

For these Hamiltonians, we obtain the corresponding current matrix elements, which we need for the evaluation of the conductivity. They are commutators with respect to the position $\mathbf{r}$ and read for MLG $j_\mu = -ie[H_M, r_\mu] = e\sigma_\mu$ and for BLG

$$j_1 = -ie[H_B, r_1] = 2e(p_1\sigma_1 + p_2\sigma_2), \quad j_2 = -ie[H_B, r_2] = 2e(-p_2\sigma_1 + p_1\sigma_2) \tag{1.13}$$

In MLG the current is the same for all momenta, whereas it is linear in the momenta for BLG. This indicates that the low-energy spectrum reveals a distinct characterization with respect to the number of graphene layers.

1.4 DC Conductivity

Transport in graphene, like in other materials, is based on the diffusion of quasiparticles. However, the situation in graphene is more subtle than in conventional

metals. First of all, graphene is a two-dimensional structure, where the scaling theory of Anderson localization for conventional metals predicts the localization of quantum states for any amount of disorder [35]. Surprisingly, this has not been confirmed by experiments. Despite the remarkable disorder effects from the substrate and from ripples in the graphene sheet, the metallic behavior is always dominant. Doping of graphene with hydrogen is one of the few exceptions, in which the material becomes nonmetallic. However, this is not due to Anderson localization but is caused by sublattice symmetry-breaking, which generates a small gap of a few meV up to 1 eV [36–38]. The reason for the absence of Anderson localization is that graphene, in contrast to a conventional metal, has two complementary bands which are connected by a particle-hole symmetry. This allows for Klein tunneling, an effect that suppresses potential scattering substantially. The particle-hole symmetry implies a chiral symmetry for the two-particle Green's function. This can be spontaneously broken by random scattering, which is indicated by a nonzero scattering rate η. Therefore, we can distinguish three different regimes: a ballistic regime with no scattering except for the sample boundaries; a diffusive regime for weak scattering; and Anderson localization for very strong scattering. Moreover, a random gap can be opened. This leads to an insulating regime for weak scattering and a metallic regime for stronger scattering and, eventually, to Anderson localization for very strong scattering.

Ballistic regime at the Dirac node: Equation 1.2 defines the diffusion coefficient in our two-band system. In the case without disorder, the correlation of Green's functions gives for the Hamiltonian in Equation 1.11

$$D = \lim_{\epsilon \to 0} \frac{1}{4\pi} \left(1 + \frac{1+\zeta^2}{\zeta} \arctan \zeta \right) \quad (\zeta = E/\epsilon) \tag{1.14}$$

This result is surprising in that it indicates diffusion at the Dirac node $E = 0$ with the diffusion coefficient $D = 1/2\pi$ even without random scattering. Away from the Dirac node ($E \neq 0$), however, D diverges, reflecting that there is no diffusion but ballistic propagation. This is accidental not only for the case for MLG, since we also get a finite D at the nodes for the BLG. This behavior reveals a characteristic transport feature at the nodes of a two-band system, which is caused by quantum fluctuations. In other words, quantum fluctuations play an important role in 2D transport at the points of band degeneracy.

Diffusive regime with weak disorder scattering: Typical disorder is due to a randomly fluctuating gap. The result of a weak scattering expansion for the correlation function in Equation 1.5 is the scaling relation [39, 40]

$$\sum_{\mathbf{r}} r_k^2 Tr_2 \langle G_{\mathbf{r}0}(E_F + i\delta) G_{0\mathbf{r}}(E_F - i\delta) \rangle_d = \frac{\eta^2}{\delta^2} \sum_{\mathbf{r}} r_k^2 Tr_2 \left[G_{0,\mathbf{r}}(E_F + i\eta) G_{0,-\mathbf{r}}(E_F - i\eta) \right]. \tag{1.15}$$

This relation is very important for the evaluation of the diffusion coefficient in Equation 1.2 and the DC conductivity in Equation 1.5, since it enables us to perform the averaging over disorder. The latter results in the substitution of δ by the scattering rate η and the prefactor δ^{-2}. The scattering rate is obtained from

disorder distribution and can either be calculated in the self-consistent Born approximation [39–41] or measured in an experiment. Then the right-hand side of the relation can be evaluated in Fourier representation and gives

$$-\frac{1}{2\pi\delta^2}\left(1+\frac{1+\zeta^2}{\zeta}\arctan\zeta\right) \quad (\zeta = E_F/\eta) \tag{1.16}$$

After inserting this expression in Equation 1.5, we obtain for the DC conductivity of MLG the simple expression

$$\sigma_{DC} = \frac{2e^2}{\pi h}\left(1+\frac{1+\zeta^2}{\zeta}\arctan\zeta\right) \tag{1.17}$$

where the fourfold spin and valley degeneracy has been implemented. This result is remarkable because it is in good agreement with experimental observation of a "V"-shaped conductivity. If we compare it with the empirical formula in Equation 1.8, we can identify the minimal conductivity $\sigma_{\min} = 4e^2/\pi h$ at the Dirac node and the monotonically increasing behavior

$$\tilde{\sigma} = \frac{2e^2}{\pi h}\left(-1+\frac{1+\zeta^2}{\zeta}\arctan\zeta\right) \sim 2\frac{e^2}{\pi h}\begin{cases}\zeta^2 & \text{for } \zeta \sim 0\\ \pi\zeta/2 & \text{for } \zeta \sim \infty\end{cases} \tag{1.18}$$

away from the Dirac node. The minimal conductivity is independent of the scattering rate, which reflects the fact that quantum fluctuations are dominant. The behavior for small ζ can be expressed by the scattering time and leads to the expression

$$\tilde{\sigma} \sim 2\frac{e^2}{\pi h}\frac{\overline{E}_F^2\tau^2}{\hbar^2} \tag{1.19}$$

On the other hand, the linear behavior of $\tilde{\sigma}$ far away from the Dirac node agrees with the classical Boltzmann calculation. This is indicative of the fact that the scattering to the second band is irrelevant in this regime.

The calculation for the DC conductivity of MLG is also applicable to BLG. The main difference is that the minimal conductivity appears with an additional factor 2 [39, 40], which is a consequence of the parabolic spectrum near the node. We will see later that this factor 2 is also crucial for the AC conductivity. Like in the case of minimal conductivity, it is not due to independent currents through the two layers but due to the spectral curvature near the nodes.

Anderson localization: Is it realistic to see Anderson localization, that is, the absence of diffusion, in graphene? In a one-band system, it is always present in two-dimensional systems, according to the scaling theory [35]. In a two-band system, this is less clear. For weak scattering, we have seen that diffusion prevails because of spontaneous breaking of chiral symmetry. For very strong scattering, when the scattering rate η exceeds the band width, we have found a transition to Anderson localization [42]. However, such strong scattering rates are rather unrealistic in graphene unless disorder is created intentionally (e.g., removing carbon atoms by bombardment with ions). The measured scattering rates are at least two orders smaller than this value (cf. Table 1.1). The schematic phase diagram for graphene is depicted in Figure 1.1.

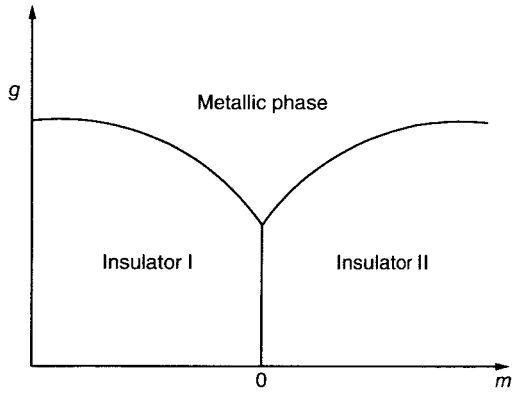

Figure 1.1 Schematic phase diagram for graphene with a random gap with average m and variance $g = \langle m^2 \rangle - \langle m \rangle^2$.

1.5 AC Conductivity for Very Weak Scattering and Thermal Fluctuations

The Kubo formula (1.6) is now employed to calculate the AC (or optical) conductivity in MLG and BLG. We assume here that $\hbar\omega \gg \eta$, so that the relevant length scale is the effective wavelength v_F/ω rather than the scattering length $v_F\tau$. This implies that disorder scattering is not important and can be neglected. Then we can treat the current matrix elements of Equation 1.13 in Fourier representation with respect to energy eigenstates $|\pm E\rangle$. Of particular interest is the matrix element that describes interband scattering, for which we obtain, after the integration over the circular Fermi surface with $E_F^2 \geq m^2$,

$$\int_0^{2\pi} |\langle E|\sigma_1|-E\rangle|^2 d\varphi = \pi\left(1+\frac{m^2}{E^2}\right) \tag{1.20}$$

in the case of MLG and

$$\int_0^{2\pi} |\langle E|k_x\sigma_1 + k_y\sigma_2|-E\rangle|^2 d\varphi = \pi\sqrt{E^2-m^2}\left(1+\frac{m^2}{E^2}\right) \tag{1.21}$$

in the case of the BLG. The integrated current matrix elements behave quite differently for MLG and BLG. In particular, without gap (i.e., $m = 0$) the expression is either constant (MLG) or increases linearly with energy (BLG).

Using the Kubo formula (1.6) and the expressions of the angular integrated current matrix elements in Equations 1.20 and 1.21, the integration over E gives for $\omega^2 \geq \Delta^2$, where $\Delta = 2m$ is the gap, the expression

$$\sigma'(\omega) = \gamma\frac{\pi e^2}{8h}\left[1+\frac{\Delta^2}{\omega^2}\right]\left[f_\beta\left(-\frac{\hbar\omega}{2}\right) - f_\beta\left(\frac{\hbar\omega}{2}\right)\right] \tag{1.22}$$

for the real part of the AC conductivity. γ is the degeneracy, with $\gamma = 4$ for MLG and $\gamma = 8$ for BLG. Thus the conductivities of MLG and BLG agree up to a factor 2. The additive correction due to the gap parameter Δ^2 decays like ω^{-2}, which resembles the intraband scattering of the Drude behavior in Equation 1.7.

In the special gapless case, $m = 0$ and $T \sim 0$, and we get for the AC conductivity $\sigma_{AC} = \sigma' + i\sigma''$ the real part

$$\sigma'(\omega) = \gamma \frac{\pi e^2}{8h} \Theta(\hbar\omega - 2E_F) \tag{1.23}$$

and the imaginary part

$$\sigma''(\omega) = \gamma \frac{e^2}{16h} \left[4\frac{E_F}{\hbar\omega} - \log\left(\left| \frac{2E_F + \hbar\omega}{2E_F - \hbar\omega} \right| \right) \right] \tag{1.24}$$

The first term resembles the Drude result in Equation 1.7, because this is a contribution from intraband scattering [43]. It should be noticed that $\sigma''(\omega)$ vanishes for $\omega \gg E_F$. If we take the full band structure of the honeycomb lattice into account, the AC conductivity deviates from the low-energy result of Equation 1.22. This is shown in Figure 1.2, where $\sigma'(\omega)$ versus the frequency is plotted. In particular, there is a characteristic conductivity maximum at the van Hove singularity, where the Fermi surfaces of the two nodes merge. The Fermi energy $E_F \neq 0$ creates a step at $\hbar\omega = 2E_F$ because excitations without momentum transfer are possible only from the Fermi sea to unoccupied states in the upper band (cf. Figure 1.3).

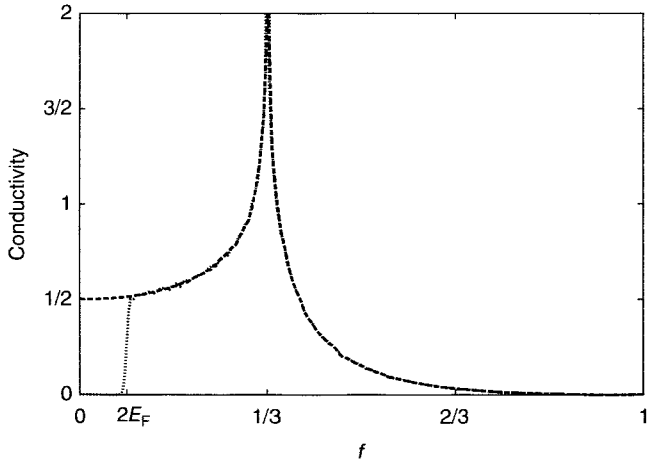

Figure 1.2 Real part of the AC conductivity at $T = 0$ in units of $\pi e^2/h$ as a function of the rescaled frequency $f = \hbar\omega/t$ for the honeycomb lattice, where $t = 2.8$ eV is the bandwidth. There is a characteristic peak due to a van Hove singularity. The Fermi energy is at the charge neutrality point $E_F = 0$ (full curve) and above the charge neutrality point at $E_F = 0.04t$ (dotted curve).

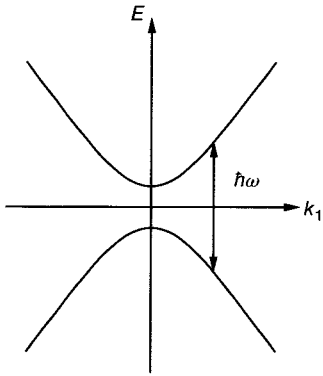

Figure 1.3 Schematic picture of the creation of an electron–hole pair in gapped MLG or BLG by the absorption of a photon with energy $\hbar\omega$. For this process, the photon energy must be larger than the bandgap $\Delta = 2m$.

The AC conductivity provides the dielectric coefficient $\epsilon(\omega)$ via the relation [5]

$$\epsilon(\omega) = 1 + \frac{4\pi i}{\omega}\sigma(\omega) \tag{1.25}$$

so that the complex dielectric coefficient reads $\epsilon = \epsilon' + i\epsilon''$ with

$$\epsilon' = 1 - \frac{4\pi}{\omega}\sigma'', \quad \epsilon'' = \frac{4\pi}{\omega}\sigma' \tag{1.26}$$

This is the dielectric function for the wave vector $\mathbf{q} = 0$: $\epsilon(\omega) = \epsilon(\mathbf{q} = 0, \omega)$. We need the dielectric function later for the description of plasmons in Section 1.6.

According to the Fresnel equations for thin layers [22, 44], the optical transmittance T is directly linked to the AC conductivity through the relation

$$T \approx \frac{1}{(1 + 2\pi\sigma'(\omega)/c)^2} \tag{1.27}$$

Using the result in Eq. 1.23, the transmittance becomes

$$T \approx 1 - \pi\alpha \quad (MLG), \quad T \approx 1 - 2\pi\alpha \quad (BLG) \tag{1.28}$$

where $\alpha = e^2/\hbar c \approx 1/137$ is the fine-structure constant. This behavior was also observed in several experiments over a wide range of frequencies [22, 23, 44].

1.6 Plasmons

Now we consider the electron gas in graphene which is subject to an external potential $V_i(\mathbf{q},\omega)$. The response of the electron gas to $V_i(\mathbf{q},\omega)$ is a screening potential $V_s(\mathbf{q},\omega)$ which is created by the rearrangement of the electrons due to the external potential. Therefore, the total potential acting on the electrons is given by

$$V(\mathbf{q},\omega) = V_i(\mathbf{q},\omega) + V_s(\mathbf{q},\omega) \tag{1.29}$$

V_s can be evaluated self-consistently [45] and is expressed via the dielectric function $\epsilon(\mathbf{q},\omega)$. Then the total potential reads [46]

$$V(\mathbf{q},\omega) = \frac{1}{\epsilon(\mathbf{q},\omega)} V_i(\mathbf{q},\omega) \tag{1.30}$$

The dielectric function can be calculated from the Lindhard formula. Assuming that the wavelength of the electromagnetic wave is much larger than the lattice spacing, the longitudinal component reads [45]

$$\epsilon(\mathbf{q},\omega) = 1 - \frac{2\pi e^2}{q}\chi(\mathbf{q},\omega) \tag{1.31}$$

where

$$\chi(\mathbf{q},\mathbf{r},\omega) = \lim_{\delta\to 0} \int_{\mathbf{k}} \sum_{l,l'=1,2} \frac{f_\beta(E_{\mathbf{k},l}) - f_\beta(E_{\mathbf{k}+\mathbf{q},l'})}{E_{\mathbf{k},l} - E_{\mathbf{k}+\mathbf{q},l'} + \hbar\omega + i\hbar\delta} |\langle \mathbf{k}+\mathbf{q},l'|e^{i\mathbf{q}\cdot\mathbf{r}}|\mathbf{k},l\rangle|^2 \tag{1.32}$$

Poles in ω of the inverse longitudinal dielectric function $1/\epsilon(\mathbf{q},\omega)$ for a given wave vector $\mathbf{q}$ correspond to the collective excitations of electrons which are called *plasmons*. These poles are located either on the real axis or in the complex plane away from the real axis. The latter can be considered as damped plasmons, which are generated by scattering with individual electrons. An imaginary term can appear in the integral $\chi(\mathbf{q},\omega)$ of Equation 1.32 if the denominator $E_{\mathbf{k}} - sE_{\mathbf{k}+\mathbf{q}} + \omega, s = \pm 1$ vanishes inside the Brillouin zone. In other words, if $(\mathbf{q},\omega)$ is inside the band that is produced by the spectrum of the electrons, that is, where an electronic wave vector $\mathbf{k}$ exists that satisfies

$$E_{\mathbf{k}+\mathbf{q}} - sE_{\mathbf{k}} = \omega \tag{1.33}$$

then scattering between plasmons and electrons is possible and will lead to the damping of plasmons. On the other hand, outside the spectrum of electrons (i.e., when there is no electron wave vector k which solves Equation 1.32), we obtain undamped plasmons.

Using the Dirac Hamiltonian from Equation 1.11 as a low-energy approximation enables us to calculate the poles of the inverse dielectric function directly [47, 48]. In this case, the plasmon dispersion follows a square-root behavior

$$\omega_P \sim cq^{1/2} \tag{1.34}$$

where the prefactor c is proportional to $\sqrt{E_F}$. The plasmon dispersion, on the other hand, depends on the spectral properties of the electrons. Therefore, deviations from Dirac cones may affect them. This can lead to a stronger damping of the electrons, since electronic excitations require lower energies on the honeycomb lattice in comparison with the linearized (Dirac) spectrum [49]. For this purpose, we plot the loss function [50]

$$Im\left(\frac{1}{\epsilon(\mathbf{q},\omega)}\right) = \frac{-\epsilon''}{\epsilon'^2 + \epsilon''^2} \tag{1.35}$$

in Figure 1.4. The peak strength varies with the momentum. In particular, if the pole is away from the real axis, it becomes a Lorentzian of width ϵ''. Thus, ϵ''

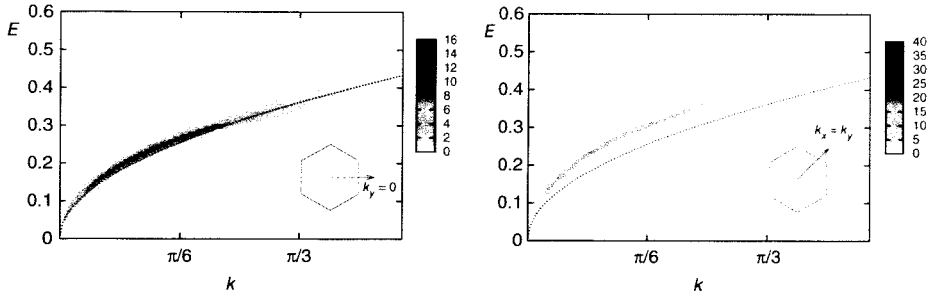

Figure 1.4 Plasmon dispersion $E = \hbar\omega/3t$ as a function of $k = q_x d$ at the Fermi energy $E_F = 0.25t$ on the honeycomb lattice (Adapted and reproduced from [49] with permission from EPL) . $d = 1.42$ Å is the lattice constant of graphene. To demonstrate the anisotropy, two different directions of the **q** vector with $q_y = 0$ (a) and $q_y = q_x$ (b) have been plotted. The isotropic square-root behavior of the Dirac case is also shown as a dashed curve.

is a measure of the damping by electron scattering. Plasmons on a honeycomb lattice with an additional next-nearest neighbor hopping have also been studied [51]. Although the additional hopping breaks the particle-hole symmetry of the two-band system, there is no drastic effect on the plasmon dispersion.

The two panels of Figure 1.4 demonstrate the anisotropy of the plasmon dispersion for electrons on the honeycomb lattice. There is a substantial deviation from the isotropic plasmon dispersion of the Dirac Hamiltonian.

The square-root behavior of the plasmon dispersion, on the other hand, is quite general for a two-dimensional electron gas. For a conventional 2D electron gas with parabolic electron dispersion with effective electron mass m, the plasmon dispersion reads [52]

$$\omega_p(q) = \frac{\sqrt{\left(4a + v_F^2 q\right) q \left(q^4 v_F^4 + 4q^3 v_F^2 a + 16 k_F^2 a^2\right)} \left(v_F^2 q + 2a\right)}{4\left(4a + v_F^2 q\right) a k_F} \tag{1.36}$$

with $a = 2ne^2/m$ and the Fermi velocity v_F. Expansion for small q then gives

$$\omega_p^2 \approx aq + \frac{3}{4} v_F^2 q^2 \tag{1.37}$$

Thus, plasmons in graphene have similar properties as those in a conventional 2D electron gas.

1.7 Discussion

Transport in graphene is remarkably different from that in conventional metals. The main reason is the scattering between the valence and the conduction band, which leads to Klein tunneling. This has several consequences for the electronic and optical properties in MLG and BLG. First of all, it creates a minimal

conductivity for the neutral system ($E_F = 0$), which can be explained by quantum fluctuations of the system without electric charges. The other distinctive feature is the constant AC conductivity over a wide range of frequencies. This was also observed in a number of experiments for frequencies ranging from infrared to visible light [22, 23]. Another characteristic feature is that the AC conductivity of BLG is twice as large as that of MLG. This was also observed experimentally with high accuracy [22]. A third important aspect is that graphene defies Anderson localization, which is possible only for very strong scattering. Therefore, diffusion is the main transport mechanism in graphene. We can conclude that the DC transport behavior of graphene becomes more conventional and Drude-like as we go deeper in the valence band (for holes) or in the conduction band (for electrons) because interband scattering becomes less important. On the other hand, exactly at the nodes of the bands the transport behavior is quite special, because the Fermi surface shrinks to a point.

References

1. Novoselov, K.S., Geim, A.K., Morozov, S.V., Jiang, D., Zhang, Y., Dubonos, S.V., Grigorieva, I.V., and Firsov, A.A. (2004) Electric field effect in atomically thin carbon films. *Science*, **306**, 666–669; (b) Novoselov, K.S., Geim, A.K., Morozov, S.V., Jiang, D., Katsnelsnon, M.I., Grigorieva, I.V., Dubonos, S.V., and Firsov, A.A. (2005) Two-dimensional gas of massless Dirac fermions in graphene. *Nature*, **438**, 197–200; (c) Zhang, Y., Tan, Y.-W., Stormer, H.L., and Kim, P. (2005) Experimental observation of the quantum Hall effect and Berry's phase in graphene. *Nature*, **438**, 201–204.
2. Castro Neto, A.H., Guinea, F., Peres, N.M.R., Novoselov, K.S., and Geim, A.K. (2009) The electronic properties of graphene. *Rev. Mod. Phys.*, **81**, 109–162.
3. Abergel, D.S.L., Apalkov, V., Berashevich, J., Ziegler, K., and Chakraborty, T. (2010) Properties of graphene: a theoretical perspective. *Adv. Phys.*, **59** (4), 261–482.
4. Andrei, E.Y., Li, G., and Du, X. (2012) Electronic properties of graphene: a perspective from scanning tunneling microscopy and magnetotransport. *Rep. Prog. Phys.*, **75** (5), 056501.
5. Ashcroft, N.W. and Mermin, N.D. (1976) *Solid State Physics*, Saunders College Publishing.
6. Ziegler, K. (2006) Robust transport properties in graphene. *Phys. Rev. Lett.*, **97**, 266802.
7. Ziegler, K. (2008) Long-range correlations in disordered graphene. *Phys. Rev. B*, **78**, 125401.
8. Hwang, E.H., Adam, S., and Das Sarma, S. (2007) Carrier transport in two-dimensional graphene layers. *Phys. Rev. Lett.*, **98**, 186806.
9. Geim, A.K. and Novoselov, K.S. (2007) The rise of graphene. *Nat. Mater.*, **6**, 183–191.
10. Tan, Y.-W., Zhang, Y., Bolotin, K., Zhao, Y., Adam, S., Hwang, E.H., Das Sarma, S., Stormer, H.L., and Kim, P. (2007) Measurement of scattering rate and minimum conductivity in graphene. *Phys. Rev. Lett.*, **99**, 246803.
11. Morozov, S.V., Novoselov, K.S., Katsnelson, M.I., Schedin, F., Elias, D.C., Jaszczak, J.A., and Geim, A.K. (2008) Giant intrinsic carrier mobilities in graphene and its bilayer. *Phys. Rev. Lett.*, **100**, 016602.
12. Chen, J.H., Jang, C., Adam, S., Fuhrer, M.S., Williams, E.D., and Ishigami, M. (2008) Charged-impurity scattering in graphene. *Nat. Phys.*, **4**, 377–381.
13. Du, X., Skachko, I., Barker, A., and Andrei, E.Y. (2008) Approaching ballistic transport in suspended graphene. *Nat. Nanotechnol.*, **3**, 491–495.

14. Danneau, R., Wu, F., Craciun, M.F., Russo, S., Tomi, M.Y., Salmilehto, J., Morpurgo, A.F., and Hakonen, P.J. (2008) Evanescent wave transport and shot noise in graphene: ballistic regime and effect of disorder. *J. Low Temp. Phys.*, **153**, 374–392.
15. Martin, J., Akerman, N., Ulbricht, G., Lohmann, T., Smet, J.H., von Klitzing, K., and Yacoby, A. (2008) Observation of electron-hole puddles in graphene using a scanning single-electron transistor. *Nat. Phys.*, **4**, 144–148.
16. Elias, D.C., Nair, R.R., Mohiuddin, T.M.G., Morozov, S.V., Blake, P., Halsall, M.P., Ferrari, A.C., Boukhvalov, D.W., Katsnelson, M.I., Geim, A.K., and Novoselov, K.S. (2009) Control of graphene's properties by reversible hydrogenation: evidence for graphane. *Science*, **323**, 610–613.
17. Herbut, I.F., Juricic, V., and Vafek, O. (2008) Coulomb interaction, ripples, and the minimal conductivity of graphene. *Phys. Rev. Lett.*, **100**, 046403.
18. Mishchenko, E.G. (2008) Minimal conductivity in graphene: interaction corrections and ultraviolet anomaly. *Europhys. Lett.*, **83**, 17005.
19. Sheehy, D.E. and Schmalian, J. (2007) Quantum critical scaling in graphene. *Phys. Rev. Lett.*, **99**, 226803.
20. Sinner, A. and Ziegler, K. (2010) Effect of the Coulomb interaction on the gap in monolayer and bilayer graphene. *Phys. Rev. B*, **82**, 165453.
21. Sheehy, D.E. and Schmalian, J. (2009) Optical transparency of graphene as determined by the fine-structure constant. *Phys. Rev. B*, **80**, 193411.
22. Nair, R.R., Blake, P., Grigorenko, A.N., Novoselov, K.S., Booth, T.J., Stauber, T., Peres, N.M.R., and Geim, A.K. (2008) Fine structure constant defines visual transparency of graphene. *Science*, **320**, 1308.
23. Li, Z.Q., Henriksen, E.A., Jiang, Z., Hao, Z., Martin, M.C., Kim, P., Stormer, H.L., and Basov, D.N. (2008) Dirac charge dynamics in graphene by infrared spectroscopy. *Nat. Phys.*, **4**, 532–535.
24. Yan, J., Zhang, Y., Kim, P., and Pinczuk, A. (2007) Electric field effect tuning of electron-phonon coupling in graphene. *Phys. Rev. Lett.*, **98**, 166802.
25. Yan, J., Henriksen, E.A., Kim, P., and Pinczuk, A. (2008) Observation of anomalous phonon softening in bilayer graphene. *Phys. Rev. Lett.*, **101**, 136804.
26. Mohiuddin, T.M.G., Lombardo, A., Nair, R.R., Bonetti, A., Savini, G., Jalil, R., Bonini, N., Basko, D.M., Galiotis, C., Marzari, N., Novoselov, K.S., Geim, A.K., and Ferrari, A.C. (2009) Uniaxial strain in graphene by Raman spectroscopy: G peak splitting, Grüneisen parameters, and sample orientation. *Phys. Rev. B*, **79**, 205433.
27. Zhang, Y., Brar, V.W., Wang, F., Girit, C., Yayon, Y., Panlasigui, M., Zettl, A., and Crommie, M.F. (2008) Giant phonon-induced conductance in scanning tunnelling spectroscopy of gate-tunable graphene. *Nat. Phys.*, **4**, 627–630.
28. Pallecchi, E., Betz, A.C., Chaste, J., Fève, G., Huard, B., Kontos, T., Berroir, J.-M., and Plaçais, B. (2011) Transport scattering time probed through rf admittance of a graphene capacitor. *Phys. Rev. B*, **83**, 125408.
29. Bostwick, A., McChesney, J.L., Emtsev, K.V., Seyller, T., Horn, K., Kevan, S.D., and Rotenberg, E. (2009) Quasiparticle transformation during a metal-insulator transition in graphene. *Phys. Rev. Lett.*, **103**, 056404.
30. Ohta, T., Bostwick, A., Seyller, T., Horn, K., and Rotenberg, E. (2006) Controlling the electronic structure of bilayer graphene. *Science*, **313**, 951–954.
31. Oostinga, J.B., Heersche, H.B., Liu, X., Morpurgo, A.F., and Vandersypen, L.M.K. (2008) Gate-induced insulating state in bilayer graphene devices. *Nat. Mater.*, **7**, 151–157.
32. Morozov, S.V., Novoselov, K.S., Katsnelson, M.I., Schedin, F.L., Ponomarenko, A., Jiang, D., and Geim, A.K. (2006) Strong suppression of weak localization in graphene. *Phys. Rev. Lett.*, **97**, 016801.
33. Meyer, J.C., Geim, A.K., Katsnelson, M.I., Novoselov, K.S., Booth, T.J., and Roth, S. (2007) The structure of suspended graphene sheets. *Nature*, **446**, 60–63.

34. McCann, E., Kechedzhi, K., Fal'ko, V.I., Suzuura, H., Ando, T., and Altshuler, B.L. (2006) Weak-localization magnetoresistance and valley symmetry in graphene. *Phys. Rev. Lett.*, **97**, 146805.
35. Abrahams, E., Anderson, P.W., Licciardello, D.C., and Ramakrishnan, T.V. (1979) Scaling theory of localization: absence of quantum diffusion in two dimensions. *Phys. Rev. Lett.*, **42**, 673–676.
36. Zhou, S.Y., Gweon, G.-H., Fedorov, A.V., First, P.N., de Heer, W.A., Lee, D.-H., Guinea, F., Castro Neto, A.H., and Lanzara, A. (2007) Substrate-induced bandgap opening in epitaxial graphene. *Nat. Mater.*, **6**, 770–775.
37. Lu, Y.H., Chen, W., Feng, Y.P., and He, P.M. (2009) Tuning the electronic structure of graphene by an organic molecule. *J. Phys. Chem. B*, **113** (1), 2–5.
38. Haberer, D., Vyalikh, D.V., Taioli, S., Dora, B., Farjam, M., Fink, J., Marchenko, D., Pichler, T., Ziegler, K., Simonucci, S., Dresselhaus, M.S., Knupfer, M., Büchner, B., and Grüneis, A. (2010) Tunable band gap in hydrogenated quasi-free-standing graphene. *Nano Lett.*, **10**, 3360–3366.
39. Ziegler, K. (2009) Random-gap model for graphene and graphene bilayers. *Phys. Rev. Lett.*, **102**, 126802.
40. Ziegler, K. (2009) Diffusion in the random gap model of monolayer and bilayer graphene. *Phys. Rev. B*, **79**, 195424.
41. Shon, N.H. and Ando, T. (1998) Quantum transport in two-dimensional graphite system. *J. Phys. Soc. Jpn.*, **67**, 2421–2429.
42. Hill, A. and Ziegler, K. (2014) Anderson localization in a two-dimensional random gap model. *Physica E*, **56**, 172–176.
43. Mikhailov, S.A. and Ziegler, K. (2007) New electromagnetic mode in graphene. *Phys. Rev. Lett.*, **99**, 016803.
44. Kuzmenko, A.B., van Heumen, E., Carbone, F., and van der Marel, D. (2008) Universal optical conductance of graphite. *Phys. Rev. Lett.*, **100**, 117401.
45. Ehrenreich, H. and Cohen, M.H. (1959) Self-consistent field approach to the many-electron problem. *Phys. Rev.*, **115**, 786–790.
46. Mahan, G. (1990) *Many Particle Physics*, Plenum Press, New York.
47. Hwang, E.H. and Das Sarma, S. (2007) Dielectric function, screening, and plasmons in two-dimensional graphene. *Phys. Rev. B*, **75**, 205418.
48. Wunsch, B., Stauber, T., Sols, F., and Guinea, F. (2006) Dynamical polarization of graphene at finite doping. *New J. Phys.*, **8**, 318.
49. Hill, A., Mikhailov, S.A., and Ziegler, K. (2009) Dielectric function and plasmons in graphene. *Europhys. Lett.*, **87**, 27005, (doi:10.1209/0295-5075/87/27005).
50. Polini, M., Asgari, R., Borghi, G., Barlas, Y., Pereg-Barnea, T., and MacDonald, A.H. (2008) Plasmons and the spectral function of graphene. *Phys. Rev. B*, **77**, 081411(R).
51. Kadirko, V., Ziegler, K., and Kogan, E. (2013) Next-nearest-neighbor tight-binding model of plasmons in graphene. *Graphene*, **2** (3), 97–101.
52. Stern, F. (1967) Polarizability of a two-dimensional electron gas. *Phys. Rev. Lett.*, **18**, 546–548.